


RESEARCH PAPER



Structure-guided design of anti-cancer ribonucleotide reductase inhibitors

Tessianna A. Misko^{a,#} , Yi-Ting Liu^{b,#}, Michael E. Harris^c, Nancy L. Oleinick^d, John Pink^e, Hsueh-Yun Lee^{b,f,*} and Chris G. Dealwis^{a,g,*}

^aDepartment of Pharmacology, School of Medicine, Case Western Reserve University, Cleveland, OH, USA; ^bSchool of Pharmacy, College of Pharmacy, Taipei Medical University, Taipei, Taiwan; ^cDepartment of Chemistry, University of Florida, Gainesville, FL, United States; ^dDepartment of Radiation Oncology, School of Medicine, Case Western Reserve University, Cleveland, OH, USA; ^eCase Comprehensive Cancer Center, School of Medicine, Case Western Reserve University, Cleveland, OH, USA; ^fPh.D Program in Biotechnology Research and Development, College of Pharmacy, Taipei Medical University, Taipei, Taiwan; ^gDepartment of Chemistry, Center for Proteomics, Case Western Reserve University, Cleveland, OH, USA

ABSTRACT

Ribonucleotide reductase (RR) catalyses the rate-limiting step of dNTP synthesis, establishing it as an important cancer target. While RR is traditionally inhibited by nucleoside-based antimetabolites, we recently discovered a naphthyl salicyl acyl hydrazone-based inhibitor (NSAH) that binds reversibly to the catalytic site (C-site). Here we report the synthesis and *in vitro* evaluation of 13 distinct compounds (TP1–13) with improved binding to hRR over NSAH (TP8), with lower K_D 's and more predicted residue interactions. Moreover, TP6 displayed the greatest growth inhibiting effect in the Panc1 pancreatic cancer cell line with an IC_{50} of 0.393 μ M. This represents more than a 2-fold improvement over NSAH, making TP6 the most potent compound against pancreatic cancer emerging from the hydrazone inhibitors. NSAH was optimised by the addition of cyclic and polar groups replacing the naphthyl moiety, which occupies the phosphate-binding pocket in the C-site, establishing a new direction in inhibitor design.

ARTICLE HISTORY

Received 25 July 2018
Revised 26 September 2018
Accepted 2 November 2018

KEYWORDS

Ribonucleotide reductase; cancer; inhibitor; pancreatic; phosphate-binding




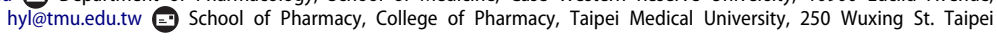
Introduction

Human ribonucleotide reductase (hRR) is a ubiquitous multi-subunit enzyme that is crucial for cell division and DNA repair^{1–4}. RR catalyses the rate-determining step of dNTP synthesis by removing the 2' hydroxyl of the ribose to generate a deoxyribose¹. RR is critical for the maintenance of a balanced nucleotide pool in cells where imbalances lead to mutator phenotypes^{1,5,6}. RR activity is maintained under tight regulation at the levels of transcription⁷, allostery¹, cellular localisation⁸, and enzyme inhibition by Sml1 in *Saccharomyces cerevisiae*⁹. hRR is a multi-subunit enzyme consisting of a large subunit hRRM1, containing a catalytic site (C-site) and two allosteric sites known as the specificity site (S-site) and the activity site (A-site)¹ (Figure 1). hRRM1 associates with the small subunit hRRM2 that houses a free radical essential for catalysis to form the holoenzyme¹⁰. ATP and dATP bind the A-site, inducing active and inactive hexamers, respectively¹¹. Binding of dGTP, dTTP, dATP, or ATP to the S-site not only induces dimerisation of hRRM1 but also acts as a selection gate, regulating the relative K_{cat}/K_m for the four NDP substrates: ADP, GDP, CDP, or UDP, respectively¹.

Due to the crucial role hRR plays in replication, it is a major target for cancer chemotherapy^{12–14}. One of the first described hRR inhibitors was hydroxyurea, which targets the di-iron cluster of the hRRM2 subunit to block catalysis^{15,16}. The most common


approach for developing inhibitors in the past few decades has involved modifying natural nucleoside substrates, resulting in the production of the clinically used drugs such as gemcitabine, fludarabine, clofarabine, and cladribine^{17–23}. Gemcitabine is a billion-dollar drug used as a front line treatment of pancreatic cancer²⁴. Gemcitabine derives its main cytotoxicity through DNA chain termination^{25,26}, irreversible inhibition of hRR^{27,28} and its interactions with several phosphate-binding proteins, such as deoxycytidine deaminase (dCMP deaminase)²⁹, thymidylate synthase³⁰, CTP-synthase^{31,32}, and topoisomerase-1^{33,34}. The chain termination activity and lack of specificity exhibited by gemcitabine and other nucleoside-based drugs contribute to the toxic side effects that patients endure^{17–22}. Thus, we have proposed that the development of a selective RR-targeted inhibitor may reduce toxic side effects and expand the therapeutic window³⁵.

Our lab has set out to discover a new class of inhibitors that has higher selectivity for hRRM1, moving away from the nucleoside-based analogues and towards reversible, competitive, non-nucleoside inhibitors. An *in silico* drug screen of 350,000 compounds from the Cincinnati chemical library (formerly the Proctor and Gamble chemical library) was performed using a human RR structure complexed with the effector TTP and the substrate GDP (PDB code 3HND)^{35,36}. From this screen came the discovery of our lead inhibitor, NSAH³⁵. Crystallographic and kinetic studies indicated that NSAH binds reversibly to the C-site of hRR and acts as

CONTACT Chris G. Dealwis  cxdl114@case.edu  Hsueh-Yun Lee  hyl@tmu.edu.tw 

[#]These authors contributed equally to this work.

^{*}These authors contributed equally to this work.

 Supplemental data for this article can be accessed [here](#).

© 2019 The Author(s). Published by Informa UK Limited, trading as Taylor & Francis Group.

This is an Open Access article distributed under the terms of the Creative Commons Attribution-NonCommercial License (<http://creativecommons.org/licenses/by-nc/4.0/>), which permits unrestricted non-commercial use, distribution, and reproduction in any medium, provided the original work is properly cited.

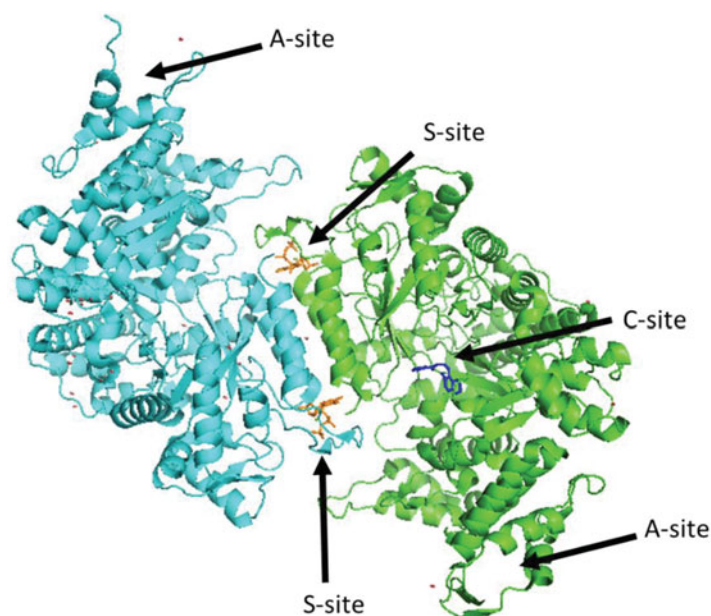


Figure 1. Structure of hRRM1 dimer.

a competitive inhibitor. The x-ray crystal structure of NSAH bound to hRRM1 was determined to 2.7 Å resolution (PDB code 5TUS)³⁵. Through chemical mimicry, NSAH occupies the space where the diphosphate ribose and base of the substrate bind in the C-site. NSAH adopts an S-shaped conformation, thermodynamically favouring the E-isomer. The crystal structure reveals that stabilisation of this conformation is due to a strong hydrogen bond between the carbonyl of NSAH and residues Ser217 and Cys218 and a hydrogen bond between the hydroxyl of the phenol of NSAH and residues Cys218 and Ser217.

This study also revealed that the salicyl acyl hydrazine moiety has a significant contributory role in the inhibitory activity against RR. NSAH inhibits cancer cell growth with IC₅₀s within two-fold of gemcitabine and leads to the depletion of deoxypurine pools, a hallmark of cellular hRR inhibition. Unlike gemcitabine, NSAH demonstrated little measurable toxicity against normal mobilised peripheral blood progenitor cells, giving NSAH a higher therapeutic index than found for gemcitabine³⁵. Nevertheless, medicinal chemistry and synthetic approaches can be used to improve the potency of NSAH and its target selectivity towards hRR. Indeed, a recent paper from our laboratory reported on a library of 25 NSAH analogues whose modifications were designed to target residues within the C-site of hRR that are important for interactions with natural substrates³⁷. These results indicated that those analogues which demonstrated a 2–4 fold improved potency of cell-free hRR over NSAH all showed hydrogen bonding with Ser606, Thr607, and Ser217, residues that are known to hydrogen bond with natural substrates.

The present study investigated the structure activity relationship of a new library of compounds to explore the chemical diversity that can target a compound to the phosphate- and ribose-binding domains within the C-site. One structure-guided approach to this goal was to modify the naphthalene ring of NSAH by dissociating the fused ring, providing a biphenyl moiety with different types of substitutions (Group 1). Furthermore, the phenyl ring was replaced by thiophene and furan using a bioisosterism strategy (Figure 2(A)). To understand the effect of the linker on RR modulation, the hydrazide group was replaced by diacylhydrazine or thiazole (shown in purple, Figure 2(A), Group 2). Meanwhile, some polar rings such as pyridine, adenine, isatin and 2-pyridone were linked by hydrazide

or diacylhydrazine to explore the structure-activity relationship. As a result, compounds **TP1-13** (Figure 2(B)) were synthesised and relevant assays to characterise their interaction with hRRM1 were conducted in this study. Using docking studies to explore possible interactions with hRRM1, it was determined that this library of compounds displayed an increase in the interactions with the phosphate-binding region of the C-site, and the best binding compounds make use of strong interactions to either the phosphate-binding region or residues near loop 2. Cancer cell studies indicated that group 1 compounds showed the greatest potency in cells, where polar substituents incorporating electronegative elements distinguished the more cytotoxic compounds. In fact, the most potent inhibitors from this class demonstrated up to a two-fold improvement in potency against the growth inhibition of pancreatic cancer cells (Panc1) relative to NSAH. The results of this study will lead to the design of future generations of compounds that further improve on target hRR inhibition and cytotoxic efficacy.

Materials and methods

Synthesis and characterisation of TP1-13

Nuclear magnetic resonance (¹H NMR and ¹³C NMR) spectra were recorded with Bruker Fourier 500 NMR spectrometers, with chemical shifts in parts per million (δ) downfield from tetramethylsilane (TMS), the internal standard (Supplemental pages S10–35). High-resolution mass spectra (HRMS) were recorded with a JEOL (JMS-700) mass spectrometer (Supplemental pages S36–48). The purities of the final compounds were determined using an Agilent 1100 series HPLC system with a C-18 column (Agilent ZORBAX Eclipse XDB-C18 5 μm, 4.6 mm × 150 mm) and were found to be ≥95%. Flash column chromatography was conducted using silica gel (Merck Kieselgel 60, No. 9385, 230 – 400 mesh ASTM). All reactions were conducted under an atmosphere of dry N₂.

(E)-2-Hydroxy-N'-(2-oxoindolin-3-ylidene)benzohydrazide (TP1)

A mixture of methyl salicylate (1.0 eq), N₂H₄ (1.1 eq), and EtOH was heated to reflux until the reaction complete. The reaction mixture was filtrated and washed with EtOH to afford a white solid. The resultant was re-suspended in EtOH, and then isatin (1.1 eq) was

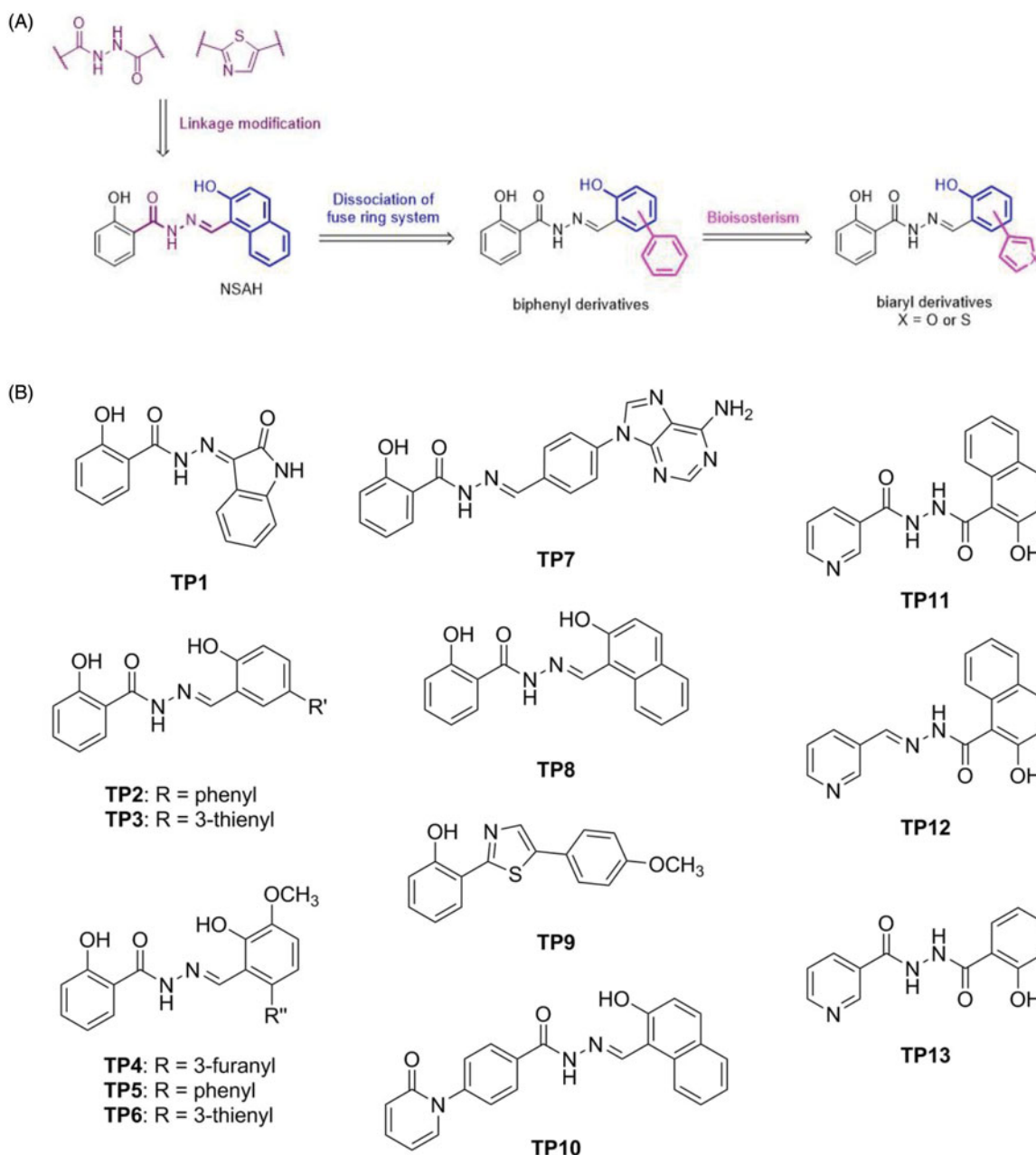


Figure 2. Schematic and structures of synthesised compounds.

added. The resulting mixture was heated to reflux until the reaction was complete (12 h). The reaction was quenched by adding H₂O and the resulting suspension was filtered and washed by EtOH to obtain **TP1** (42%). mp = 320.4 °C (decomposed); ¹H NMR (500 MHz, DMSO-*d*₆) δ 6.92 (d, *J* = 8.0 Hz, 1H), 6.97 (t, *J* = 8.0 Hz, 1H), 7.01 (d, *J* = 8.5 Hz, 1H), 7.08 (t, *J* = 8.0 Hz, 1H), 7.35 (dt, *J* = 1.0, 8.0 Hz, 1H), 7.44 (dt, *J* = 1.5, 8.5 Hz, 1H), 7.57 (d, *J* = 7.5 Hz, 1H), 7.97 (dd, 1.0, 7.5 Hz, 1H), 11.13 (s, 1H), 11.64 (s, 1H), 14.35 (s, 1H). ¹³C NMR (125 MHz, DMSO-*d*₆) δ 111.34, 111.59, 115.75, 117.28, 117.51, 117.87, 120.14, 120.71, 120.95, 121.23, 122.35, 122.86, 124.17, 131.82, 131.85, 131.94, 133.26, 134.70, 134.93, 137.49, 139.03, 142.86, 144.35, 156.51, 157.14, 162.03, 163.36, 165.28. HRMS (ESI) for C₁₅H₁₂N₃O₃ [M + H]⁺ calculated 282.0879, found 282.0880.

(E)-2-Hydroxy-N'-((4-hydroxy-[1,1'-biphenyl]-3-yl)methylene)-benzohydrazide (TP2)

The title compound was obtained in 63% overall yield from compound **14** in a manner similar to that described for the

preparation of **TP1** (reaction time: 12 h): mp = 273.5–274.9 °C; ¹H NMR (500 MHz, DMSO-*d*₆) δ 6.96–7.01 (m, 2H), 7.05 (d, *J* = 8.5 Hz, 1H), 7.32 (t, *J* = 7.5 Hz, 1H), 7.43–7.48 (m, 3H), 7.62–7.65 (m, 3H), 7.88 (d, *J* = 2.0 Hz, 1H), 7.91 (dd, *J* = 1.0, 8.0 Hz, 1H), 8.76 (s, 1H), 11.34 (s, 1H), 11.80–11.86 (m, 1H), 12.11 (s, 1H). ¹³C NMR (125 MHz, DMSO-*d*₆) δ 116.15, 117.54, 117.78, 119.49, 126.62, 127.34, 127.77, 129.09, 129.37, 130.37, 132.00, 134.45, 139.90, 149.23, 157.61, 159.50, 165.07. HRMS (ESI) for C₂₀H₁₇N₂O₃ [M + H]⁺ calculated 333.1239, found 333.1241.

(E)-2-Hydroxy-N'-(2-hydroxy-5-(thiophen-3-yl)-benzylidene)-benzohydrazide (TP3)

The title compound was obtained in 70% overall yield from compound **14** in a manner similar to that described for the preparation of **TP1** (reaction time: 12 h): mp = 282.9–284.6 °C; ¹H NMR (500 MHz, DMSO-*d*₆) δ 6.96–7.01 (m, 3H), 7.46 (dt, *J* = 1.0, 8.0 Hz, 1H), 7.52 (d, *J* = 5.0 Hz, 1H), 7.61 (dd, *J* = 3.0, 4.5 Hz, 1H), 7.67 (dd,

$J=2.0, 8.5\text{ Hz, 1H}$), 7.75 (d, $J=1.5\text{ Hz, 1H}$), 7.88–7.92 (m, 2H), 8.72 (s, 1H), 11.33 (s, 1H), 11.86–12.08 (m, 2H). ^{13}C NMR (125 MHz, DMSO- d_6) δ 116.17, 117.43, 117.78, 119.27, 119.49, 120.01, 126.47, 127.31, 127.45, 129.10, 129.97, 134.45, 141.22, 149.35, 157.24, 159.46, 165.05. HRMS (ESI) for $\text{C}_{18}\text{H}_{15}\text{N}_2\text{O}_3\text{S}$ $[\text{M} + \text{H}]^+$ calculated 339.0803, found 339.0804.

(E)-N'-(6-(furan-3-yl)-2-hydroxy-3-methoxybenzylidene)-2-hydroxybenzohydrazide (TP4)

The title compound was obtained in 61% overall yield from compound **14** in a manner similar to that described for the preparation of **TP1** (reaction time: 12 h): mp = 228.3 °C (decomposed); ^1H NMR (500 MHz, DMSO- d_6) δ 3.83 (s, 3H), 6.70 (s, 1H), 6.84 (d, $J=8.0\text{ Hz, 1H}$), 6.94–6.99 (m, 2H), 7.09 (d, $J=8.5\text{ Hz, 1H}$), 7.44–7.48 (m, 1H), 7.81–7.85 (m, 3H), 8.79 (s, 1H), 11.71 (s, 1H), 12.18 (s, 1H), 12.51 (s, 1H). ^{13}C NMR (125 MHz, DMSO- d_6) δ 56.37, 112.98, 114.89, 115.62, 115.69, 117.84, 119.38, 120.65, 123.60, 126.44, 128.73, 134.61, 141.32, 143.96, 147.82, 149.33, 150.38, 159.79, 165.18. HRMS (ESI) for $\text{C}_{19}\text{H}_{17}\text{N}_2\text{O}_5$ $[\text{M} + \text{H}]^+$ calculated 353.1137, found 353.1139.

(E)-2-Hydroxy-N'-((3-hydroxy-4-methoxy-[1,1'-biphenyl]-2-yl)methylene)-benzohydrazide (TP5)

The title compound was obtained in 58% overall yield from compound **14** in a manner similar to that described for the preparation of **TP1** (reaction time: 12 h): mp = 257.9 – 259.4 °C; ^1H NMR (500 MHz, DMSO- d_6) δ 3.85 (s, 3H), 6.77 (d, $J=8.0\text{ Hz, 1H}$), 6.91 (t, $J=7.5\text{ Hz, 1H}$), 6.94 (d, $J=8.5\text{ Hz, 1H}$), 7.12 (d, $J=8.5\text{ Hz, 1H}$), 7.34–7.37 (m, 2H), 7.42–7.51 (m, 4H), 7.78 (dd, $J=1.0, 8.0\text{ Hz, 1H}$), 8.54 (s, 1H), 11.64 (s, 1H), 12.16 (s, 1H), 12.56 (s, 1H). ^{13}C NMR (125 MHz, DMSO- d_6) δ 56.39, 114.70, 115.34, 115.61, 117.82, 119.31, 120.82, 127.77, 128.67, 128.91, 130.36, 134.59, 135.97, 139.53, 147.90, 149.22, 150.16, 159.84, 165.30. HRMS (ESI) for $\text{C}_{21}\text{H}_{19}\text{N}_2\text{O}_4$ $[\text{M} + \text{H}]^+$ calculated 363.1345, found 363.1347.

(E)-2-Hydroxy-N'-(2-hydroxy-3-methoxy-6-(thiophen-3-yl)benzylidene)-benzohydrazide (TP6)

The title compound was obtained in 75% overall yield from compound **14** in a manner similar to that described for the preparation of **TP1** (reaction time: 12 h): mp = 229.5 °C; ^1H NMR (500 MHz, DMSO- d_6) δ 3.83 (s, 3H), 6.82 (d, $J=8.5\text{ Hz, 1H}$), 6.91–6.97 (m, 2H), 7.08 (d, $J=8.5\text{ Hz, 1H}$), 7.20 (d, $J=5.0\text{ Hz, 1H}$), 7.44 (dt, $J=1.5, 8.5\text{ Hz, 1H}$), 7.52 (d, $J=1.5\text{ Hz, 1H}$), 7.67 (dd, $J=3.0, 5.0\text{ Hz, 1H}$), 7.81 (d, $J=8.0\text{ Hz, 1H}$), 8.67 (s, 1H), 11.69 (s, 1H), 12.19 (s, 1H), 12.55 (s, 1H). ^{13}C NMR (125 MHz, DMSO- d_6) δ 56.39, 114.72, 115.60, 115.64, 117.84, 119.35, 120.78, 124.66, 126.79, 128.71, 130.09, 130.63, 134.60, 139.82, 147.87, 149.24, 150.29, 159.83, 165.27. HRMS (ESI) for $\text{C}_{19}\text{H}_{16}\text{N}_2\text{NaO}_4\text{S}$ $[\text{M} + \text{Na}]^+$ calculated 391.0728, found 391.0731.

(E)-N'-(4-(6-amino-9H-purin-9-yl)benzylidene)-2-hydroxybenzohydrazide (TP7)

The title compound was obtained in 33% overall yield from compound **14** in a manner similar to that described for the preparation of **TP1** (reaction time: 12 h): mp = 229.5 °C; ^1H NMR (500 MHz, DMSO- d_6) δ 6.95–7.01 (m, 2H), 7.41–7.47 (m, 3H), 7.90–7.97 (m, 3H), 8.08 (d, $J=8.5\text{ Hz, 2H}$), 8.25 (s, 1H), 8.54 (s, 1H), 8.68 (s, 1H), 11.79 (s, 1H), 11.91 (s, 1H). ^{13}C NMR (125 MHz, DMSO- d_6) δ 116.55, 117.74, 119.46, 119.88, 123.27, 128.74, 129.13, 133.39,

134.29, 137.00, 139.87, 148.14, 149.60, 153.73, 156.86, 159.38, 165.21. HRMS (ESI) for $\text{C}_{19}\text{H}_{16}\text{N}_7\text{O}_2$ $[\text{M} + \text{H}]^+$ calculated 374.1365, found 374.1367.

(E)-2-Hydroxy-N'-((2-hydroxynaphthalen-1-yl)methylene)-benzohydrazide (TP8)

The title compound was obtained in 78% overall yield from compound **14** in a manner similar to that described for the preparation of **TP1** (reaction time: 12 h): mp = 223.8 °C; ^1H NMR (500 MHz, DMSO- d_6) δ 6.97–7.04 (m, 2H), 7.23 (d, $J=9.0\text{ Hz, 1H}$), 7.38–7.42 (m, 1H), 7.46 (t, $J=7.5\text{ Hz, 1H}$), 7.59 (t, $J=8.0\text{ Hz, 1H}$), 7.87 (d, $J=8.0\text{ Hz, 1H}$), 7.91–7.94 (m, 2H), 8.30 (d, $J=8.5\text{ Hz, 1H}$), 9.54 (s, 1H), 11.93 (s, 2H), 12.73 (s, 1H). ^{13}C NMR (125 MHz, DMSO- d_6) δ 109.08, 116.17, 117.79, 119.37, 119.61, 121.43, 124.03, 128.21, 128.29, 129.24, 129.40, 132.18, 133.39, 134.49, 148.17, 158.62, 159.29, 164.48. HRMS (ESI) for $\text{C}_{18}\text{H}_{15}\text{N}_2\text{O}_3$ $[\text{M} + \text{H}]^+$ calculated 307.1083, found 307.1085.

2-(5-(4-Methoxyphenyl)thiazol-2-yl)-phenol (TP9)

A mixture of 2-hydroxybenzonitrile (1.0 eq), *O,O*-diethyl dithiophosphate (2.0 eq), and H_2O was stirred at 80 °C until reaction was complete (4 h). The reaction mixture was cooled, quenched with saturated NaHCO_3 , and extracted by ethyl acetate (3 times). The organic layer was collected and dried under reduced pressure. The resulting residue was dissolved in EtOH, and then 4-methoxyphenacyl bromide (1.0 eq) was added. The mixture was heated to reflux until the reaction was complete (4 h). The solvent was removed under reduced pressure. The resulting residue was purified by recrystallization with hexane and MeOH to afford a white solid **TP9** (63%). mp = 95.2 – 96.8 °C; ^1H NMR (500 MHz, DMSO- d_6) δ 3.84 (s, 3H), 6.94 (dt, $J=1.0, 8.0\text{ Hz, 1H}$), 7.00–7.03 (m, 3H), 7.33 (dt, $J=1.0, 7.5\text{ Hz, 1H}$), 7.64 (s, 1H), 7.77 (dd, $J=1.0, 7.5\text{ Hz, 1H}$), 7.84 (d, $J=9.0\text{ Hz, 2H}$), 11.30 (s, 1H). ^{13}C NMR (125 MHz, DMSO- d_6) δ 54.41, 109.78, 113.91, 116.96, 117.10, 119.32, 126.18, 126.94, 127.10, 131.36, 154.01, 156.33, 160.15, 168.19. HRMS (ESI) for $\text{C}_{16}\text{H}_{14}\text{NO}_2\text{S}$ $[\text{M} + \text{H}]^+$ calculated 284.0745, found 284.0748.

(E)-N'-((2-Hydroxynaphthalen-1-yl)methylene)-4-(2-oxopyridin-1(2H)-yl)-benzohydrazide (TP10)

The title compound was obtained in 40% overall yield from compound **14** in a manner similar to that described for the preparation of **TP1** (reaction time: 12 h): mp = 258.6 °C; ^1H NMR (500 MHz, DMSO- d_6) δ 6.36 (t, $J=6.5\text{ Hz, 1H}$), 6.52 (d, $J=9.0\text{ Hz, 1H}$), 7.25 (d, $J=9.0\text{ Hz, 1H}$), 7.42 (t, $J=7.5\text{ Hz, 1H}$), 7.54 (t, $J=7.5\text{ Hz, 1H}$), 7.60–7.73 (m, 4H), 7.90 (d, $J=8.0\text{ Hz, 1H}$), 7.94 (d, $J=9.0\text{ Hz, 1H}$), 8.12 (d, $J=8.0\text{ Hz, 2H}$), 8.26 (d, $J=8.0\text{ Hz, 1H}$), 9.54 (s, 1H), 12.36 (s, 1H), 12.73 (s, 1H). ^{13}C NMR (125 MHz, DMSO- d_6) δ 106.34, 109.02, 119.37, 121.11, 121.18, 124.04, 127.53, 128.28, 128.31, 128.89, 129.46, 132.11, 132.69, 133.31, 139.12, 141.29, 144.13, 147.63, 158.55, 161.51, 162.20. HRMS (ESI) for $\text{C}_{23}\text{H}_{18}\text{N}_3\text{O}_3$ $[\text{M} + \text{H}]^+$ calculated 384.1348, found 384.1351.

N'-(2-Hydroxy-1-naphthoyl)-nicotinohydrazide (TP11)

The title compound was obtained in 55% overall yield from compound **14** in a manner similar to that described for the preparation of **TP1** (reaction time: 3 h): mp = 227.1 – 228.6 °C; ^1H NMR (500 MHz, DMSO- d_6) δ 7.04 (d, $J=7.5\text{ Hz, 1H}$), 7.13 (d, $J=8.5\text{ Hz, 1H}$), 7.35 (d, $J=9.0\text{ Hz, 1H}$), 7.41 (t, $J=7.5\text{ Hz, 1H}$), 7.49 (dt, $J=1.5,$

9.0 Hz, 1H), 7.54 (dt, $J=1.0, 8.0$ Hz, 1H), 7.88 (dd, $J=1.5, 7.5$ Hz, 1H), 7.94 (d, $J=8.0$ Hz, 1H), 7.97 (d, $J=8.5$ Hz, 1H), 8.08 (d, $J=9.0$ Hz, 1H), 10.41 (s, 1H), 10.80 (s, 1H). ^{13}C NMR (125 MHz, DMSO- d_6) δ 103.07, 110.14, 117.64, 118.82, 120.29, 123.72, 124.17, 128.05, 128.58, 128.97, 129.26, 132.65, 133.94, 134.20, 156.83, 157.04, 161.88, 164.22. HRMS (ESI) for $\text{C}_{17}\text{H}_{13}\text{N}_3\text{NaO}_3$ [$\text{M} + \text{Na}$] $^+$ calculated 330.0855, found 330.0850.

(E)-2-Hydroxy-N'-(pyridin-3-ylmethylene)-1-naphthohydrazide (TP12)

The title compound was obtained in 45% overall yield from compound **14** in a manner similar to that described for the preparation of **TP1** (reaction time: 6 h): mp = 202.8–204.5 °C; ^1H NMR (500 MHz, DMSO- d_6) δ 7.18 (d, $J=9.0$ Hz, 1H), 7.31 (d, $J=7.5$ Hz, 1H), 7.44–7.50 (m, 2H), 7.78 (d, $J=8.0$ Hz, 1H), 7.82–7.86 (m, 2H), 8.22 (s, 1H), 8.35 (d, $J=8.0$ Hz, 1H), 8.54 (d, $J=4.0$ Hz, 1H), 8.85 (s, 1H). ^{13}C NMR (125 MHz, DMSO- d_6) δ 114.48, 117.49, 123.11, 123.21, 124.14, 127.15, 127.92, 128.22, 130.92, 131.65, 132.00, 134.76, 145.03, 148.45, 149.99, 153.14, 166.39. HRMS (ESI) for $\text{C}_{17}\text{H}_{14}\text{N}_3\text{O}_2$ [$\text{M} + \text{H}$] $^+$ calculated 292.1086, found 292.1088.

N'-(2-Hydroxybenzoyl)-nicotinohydrazide (TP13)

A mixture of methyl salicylate (1.0 eq), N_2H_4 (1.1 eq), and EtOH was heated to reflux until the reaction was complete (2 h). The reaction mixture was filtered and washed with EtOH to afford a white solid. To a mixture of the resulting product (1.0 eq), K_2CO_3 (1.2 eq) and *p*-dioxane nicotinoyl chloride (1.2 eq) was added and the resultant mixture was heated at 40 °C until the reaction was complete (4 h). The reaction mixture was quenched with H_2O and extracted by ethyl acetate (3 times). The organic layer was collected, dried over MgSO_4 , and filtered. The resulting filtrate was dried under reduced pressure to obtain **TP13** as a white solid (75%). mp = 216.6–217.7 °C; ^1H NMR (500 MHz, DMSO- d_6) δ 6.95–7.00 (m, 2H), 7.46 (t, $J=7.5$ Hz, 1H), 7.57 (dd, $J=5.0, 8.0$ Hz, 1H), 7.92 (d, $J=7.0$ Hz, 1H), 8.26 (d, $J=8.0$ Hz, 1H), 8.78 (d, $J=4.0$ Hz, 1H), 9.08 (d, $J=1.0$ Hz, 1H), 10.73 (s, 1H), 10.90 (s, 1H), 11.83 (s, 1H). ^{13}C NMR (125 MHz, DMSO- d_6) δ 115.18, 117.84, 119.59, 124.19, 128.51, 128.94, 134.66, 135.75, 148.93, 153.06, 159.53, 164.62, 167.91. HRMS (ESI) for $\text{C}_{13}\text{H}_{12}\text{N}_3\text{O}_3$ [$\text{M} + \text{H}$] $^+$ calcd 258.0879, found 258.0880.

Compound preparation and solubility determination

For each compound, stock solutions were made in 100% DMSO to assure full solubility. Spectra of standard solutions in 100% acetonitrile were taken using UV spectroscopy. An extinction coefficient was calculated from the plot of the absorbance vs drug concentration using Beer's law (Supplemental Table 1).

K_D values were determined in K_D buffer [50 mM TRIS, pH 8.0, 5 mM MgCl_2 , 5% glycerol and 10 mM DTT]. Because the solubility of the compounds was limited in this buffer, the solubility was empirically determined as follows. Increasing amounts of a compound were dissolved in 1.5 ml of K_D buffer. The solutions were mixed by vortex and centrifuged at $5000\times g$ for 10 min, and the supernatant was promptly removed and absorbance measured by UV/Vis spectrophotometry. Using the extinction coefficients, the concentration of soluble drug was calculated for each total concentration (Supplemental Figure 1). Drug solubility measurements were carried out in duplicate. Plots of measured vs predicted concentrations were plotted in Origin graphing software. Samples

having precipitates that did not pellet were excluded from the list of 13 compounds examined in this manuscript.

Protein expression and purification of hRRM1

The hRRM1 protein was expressed in *Escherichia coli* BL21-codon plus (DE3)-RIL cells and purified using a peptide affinity column, as previously described in Fairman *et al.*³⁸. The homogenous protein was pooled and concentrated to 0.2 mg/mL, quantified using UV spectroscopy.

K_D determination by fluorescence quenching

The dissociation constant (K_D) was measured for each of the compounds using a tryptophan fluorescence quenching assay, as described previously with hRRM1 at 0.2 mg/mL³⁶. Tryptophan fluorescence spectra of hRRM1 were measured using a Horiba Fluoromax-4, 1155D-3113 FM spectrophotometer after exciting the sample at 295 nm. A background spectrum was recorded with protein in K_D buffer followed by the incremental addition of compounds (0–150 μM) at room temperature. The data were fitted in Origin graphing software using a quadratic form of the equilibrium binding equation

$$y = \frac{A \left((c+x+K) - \left((c+x+K)^2 - \sqrt{4cx} \right) \right)}{2c},$$

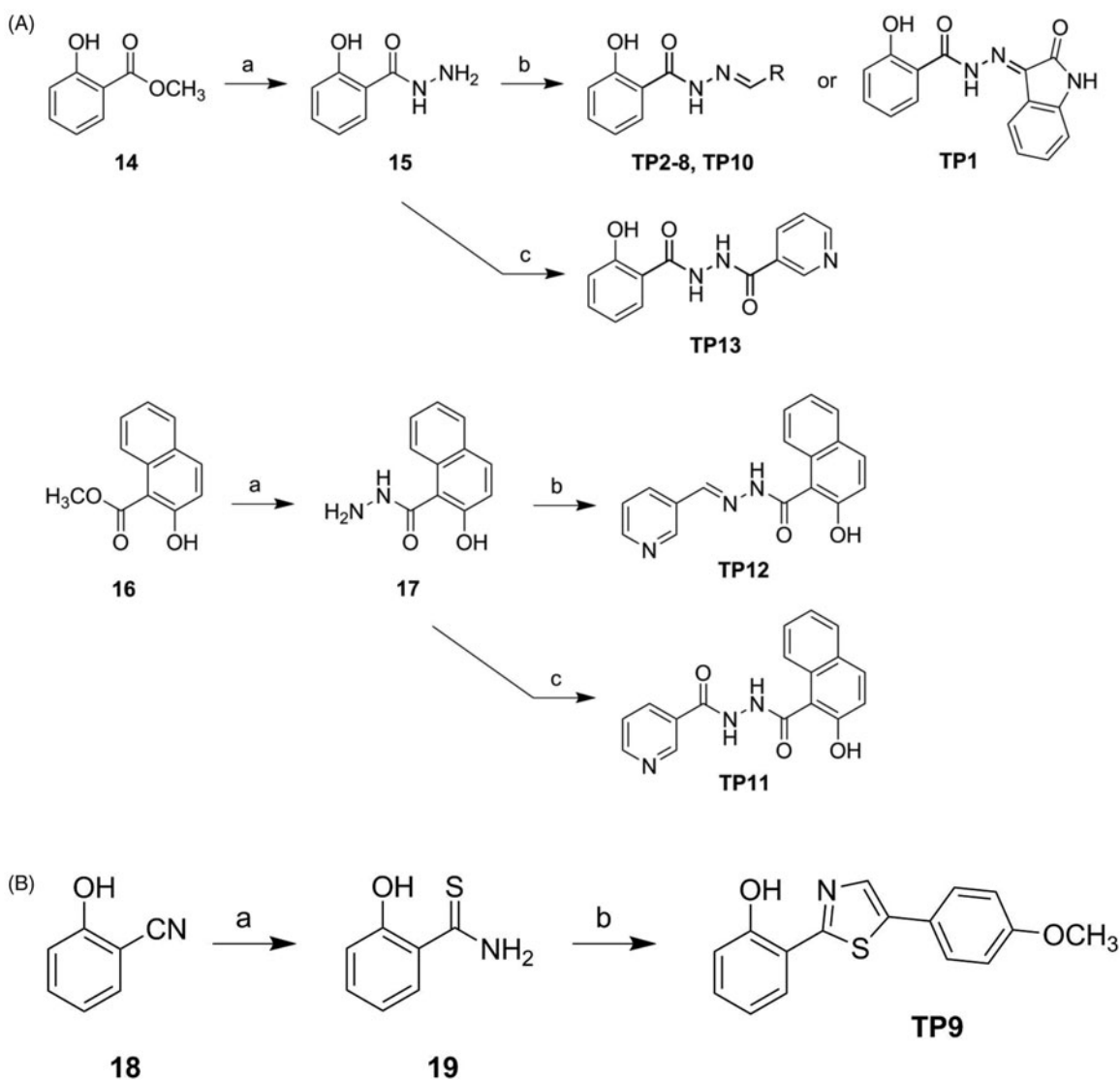
where A is the amplitude of the reaction, c is the concentration of enzyme, x is the substrate concentration, y is the percent of fluorescence quenching and K is the K_D . Measurements were made in duplicate to estimate error. K_D 's were corrected for the measured concentration of soluble compound from the concentration of total added compound. Error of the corrected K_D 's were calculated using the error propagation equation

$$\frac{\sigma_x}{x} = \sqrt{\left(\frac{\sigma_a}{a}\right)^2 + \left(\frac{\sigma_b}{b}\right)^2}$$

Where σ_x is the error of the corrected K_D , x is the corrected K_D , σ_a is the error of the slope of the drug concentration plot, a is the slope of the drug concentration plot, σ_b is the error of the measured K_D and b is the measured K_D .

Cancer cell line growth inhibition assay

Growth inhibition assays were performed in the Translational Research Shared Resource of the Case Comprehensive Cancer Centre. Human pancreatic cancer cells (Panc1) were maintained in standard growth medium consisting of (RPMI1640 + 10% FBS + 2 mM glutamine + 100 U/mL penicillin, and 100 $\mu\text{g}/\text{mL}$ streptomycin). Cells were monitored and shown to be negative for mycoplasma contamination using the Mycoplasma Detection kit (MycoAlertTM, Lonza, Basel, Switzerland). For growth inhibition assays, cells were harvested by trypsinisation and seeded into 96-well tissue culture plates at 2500 cells/mL. The following day, triplicate wells were treated with an appropriate volume of 5x-inhibitor-containing medium. The cells were cultured for 3 additional days at 37 °C in a 5% CO_2 humidified incubator. Cell growth was assessed by measuring total DNA content per well using an adaptation of the method of Labarca and Paigen³⁹.



Scheme 1. Synthetic approach to compounds TP1–13.

In silico docking studies

In silico docking of the compounds was performed using the Glide module of the Schrödinger 2017–3 modelling software suite as previously described^{36,40–42}. The docking site for the C-site was defined as a 5 Å box centred on the lead compound NSAH (TP8) bound to the hRRM1 (PDB code 5TUS)³⁷. Compounds were docked to the C-site using Glide SP. Hits were scored by a glide scoring function and examined for their interactions with the C-site residues using Maestro.

Results

Rationale for compound design and synthesis

Our previous study identified NSAH (TP8), containing a 2-hydroxybenzohydrazide moiety, as an RR modulator. Its structure contains three parts, namely: 2-hydroxybenzoyl group, hydrazide linkage, and naphthalene ring. In order to understand structure-activity relationships, specifically the influence of the hydrazide moiety, we designed diacylhydrazine-containing TP11 and TP13 and thiazole derivative TP9 (Figure 2(B)). Furthermore, hydrazide derivatives (TP1-8, TP10 and TP12) linked with biaryls or various

heterocycles were also designed. Their syntheses are illustrated in Scheme 1A and 1B. Methyl salicylate (14) was reacted with hydrazine to obtain 2-hydroxybenzohydrazide (15) which was subjected to reaction with various aldehydes or isatin to give the corresponding products TP1-8 and TP10 (Figure 2(B)). Methyl 2-hydroxy-1-naphthoate (16) underwent a similar synthetic route to afford compound TP12 (Figure 2(B)). Meanwhile, the reaction of 15 and 17 with nicotinoyl chloride yielded, respectively, compounds TP13 and TP11, which possess a diacylhydrazine linkage (Figure 2(B)). The reaction of 2-hydroxybenzonitrile (18) with *O,O*-diethyl dithiophosphate, which generated the corresponding thioamide product, was followed by cyclisation with 4-methoxyphenacyl bromide to furnish compound TP9. These analogues were designed to enhance interactions with the C-site (Figure 1).

In silico compound docking interactions with hRRM1

Potential interactions of TP1-13 with hRRM1 were investigated using the Schrödinger docking software suite glide^{40–42}. A hRRM1 dimer with lead compound NSAH bound to the C-site (PDB ID: 5TUS) was used as a model for the docking of the new compounds³⁵. It was assumed that the primary site of binding for these compounds would be the C-site, because NSAH and all previously

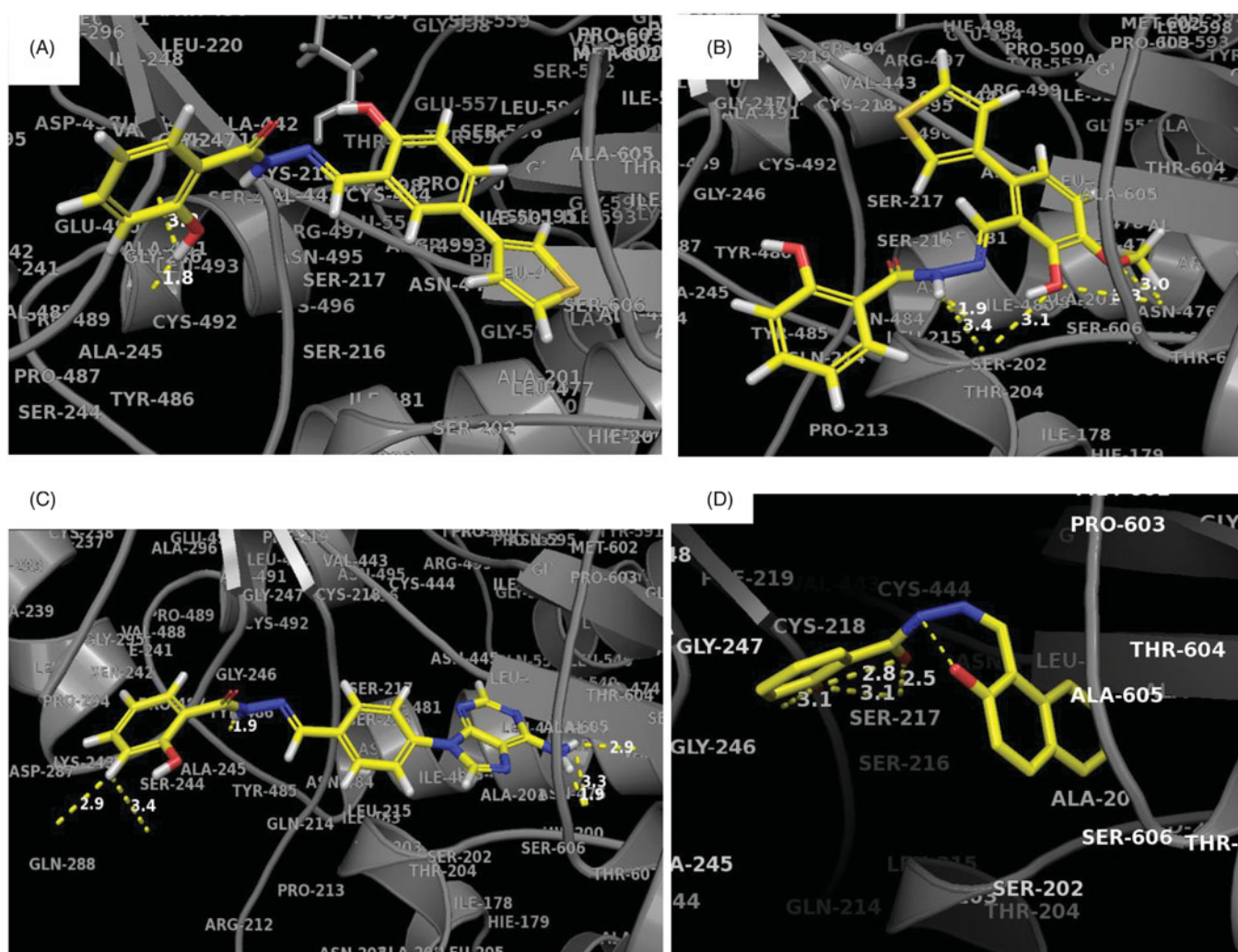


Figure 3. Predicted binding interactions of TP compounds at the C-site of hRRM1.

studied derivatives of NSAH have demonstrated a preference for the C-site^{35,37}. Our studies showed that compounds **TP2–7, 9–10** are longer and therefore extend beyond NSAH, allowing for the possibility of more interactions (Figure 3(A–D) and Supplemental Figure 1(B–F)). **TP3** was not predicted to bind well to the phosphate-binding site in comparison to other new compounds (Figure 3(A), Supplemental Figure 2(C)). However, docking predicted it to have an increase in the number of strong interactions closer to the loop 2 region. **TP7** was unique in that it was predicted to interact strongly in the phosphate-binding site with the residues: Thr607, Ser448, Ser606, and near the loop 2 region with residues: Pro294, Ala245, as well as to a residue to which NSAH exhibits strong hydrogen bonding (Ser217) (Figure 3(C), Supplemental Figure 2(G)). This is partly because **TP7** extends to the outer extremities of the catalytic site (C-site). Thus, for all compounds except **TP3**, there was either an increase in the number of predicted C-site interactions and/or an increase in the number of strong binding interactions to the phosphate-binding site of the C-site, in comparison to the interactions that NSAH makes (Figures 3(A–D), Supplemental Figure 1(A–I), Supplemental Figure 2(A–M)).

Investigation of compound binding to hRRM1 using intrinsic tryptophan fluorescence

TP1–13 were analysed for their ability to bind to hRRM1 and therefore quench its intrinsic tryptophan fluorescence. Using the criterion

that ligands quenching at least 25% of the fluorescence have sufficient affinity for hRRM1, **TP1–13** were characterised as binders of hRRM1. **TP1, 4, 6, 7, 10,** and **12** quenched at least 90% of the tryptophan fluorescence (Figure 4(A–B)). **TP2, 5, 8, 9, 11,** and **13** each quenched approximately 80% (Figure 4(C)), and **TP3** quenched approximately 70% of tryptophan fluorescence. While percentage of quenching indicates the ability of a compound to bind to the enzyme, measuring the concentration of a compound needed to quench the fluorescence by half provides the K_D , a measure of the affinity of a compound for the enzyme. Corrected K_D 's (see Methods) ranged from $2.9 \pm 0.39 - 22.0 \pm 5.67 \mu\text{M}$, where all of the new compounds have a lower K_D than NSAH ($22.0 \pm 5.67 \mu\text{M}$) (Table 1). The reduction in the K_D indicates that the chemical modifications targeting the phosphate-binding site and loop 2 resulted in better binding to hRRM1 as compared to NSAH (Table 1).

Inhibition of growth of Panc1 pancreatic cancer cells

Since gemcitabine is a core component of the current standard of care for pancreatic cancer, and we hoped to improve upon the therapeutic index for drugs treating this disease, we selected Panc1, a cell line derived from pancreatic cancer, for the study of the new compounds. Panc1 cells growing in 96-well plates were exposed to each compound continuously for three days, after which DNA content per well was measured as an indicator of cell growth. As shown in Figure 5 and Table 1, **TP1, 7, 9, 11, 12,** and

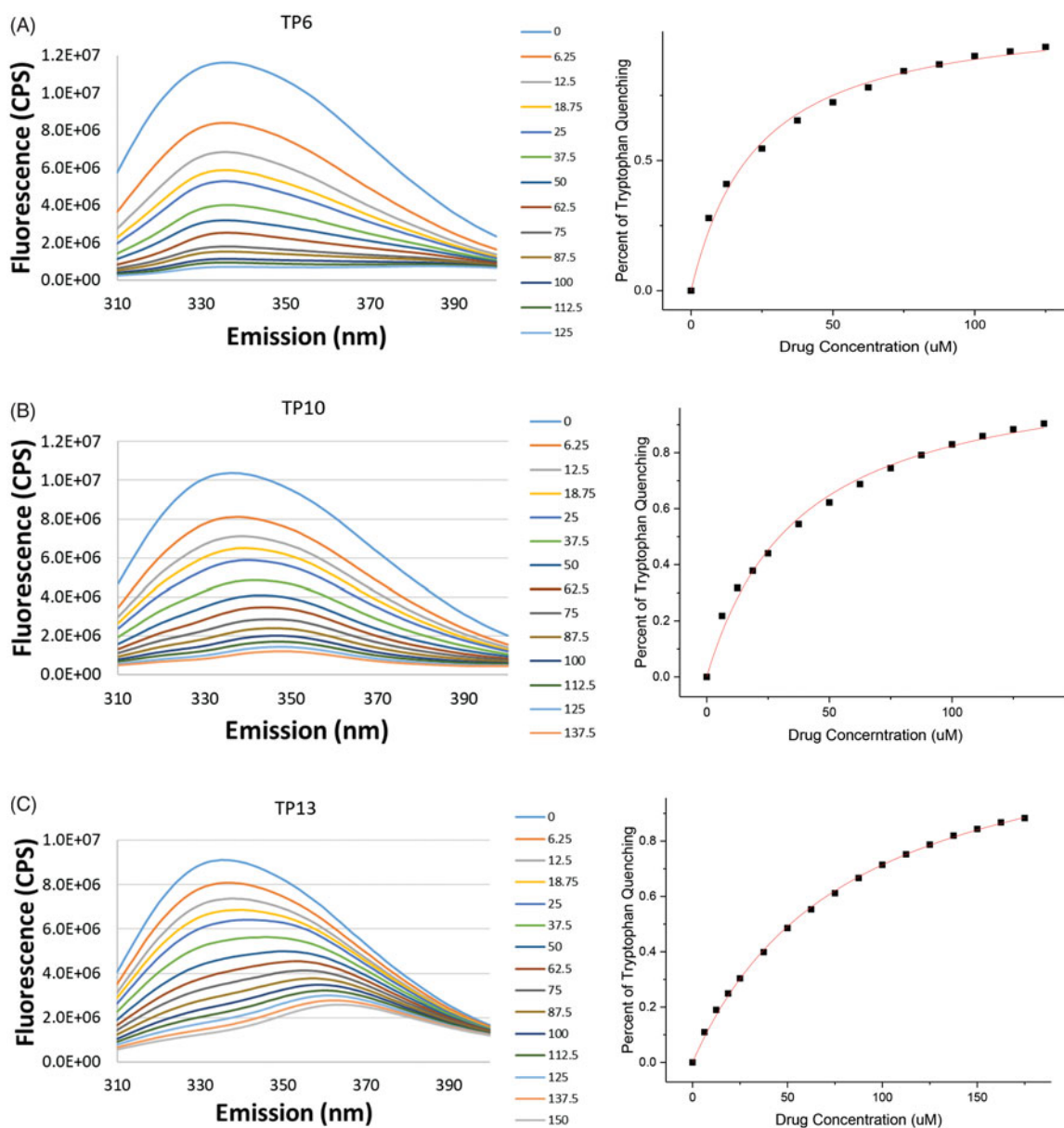


Figure 4. Quenching of tryptophan fluorescence of hRRM1 by TP ligands.

13 did not inhibit the growth of Panc1 cells, even at concentrations of $10\ \mu\text{M}$. Compounds **TP2**, **3**, and **10** showed moderate growth inhibition with IC_{50} 's between 2 and $3\ \mu\text{M}$ (Figure 5 and Table 1). Compounds **TP4–6**, and **8** were the most potent against this cell line, with IC_{50} 's below $1.5\ \mu\text{M}$ (Figure 5 and Table 1). Overall, the results indicated that some compounds in group 1 have marked activity against the growth of Panc1 cells, whereas group 2 is mostly ineffective (Figure 5 and Table 1). **TP6** demonstrated the greatest potency, with over a 2-fold decrease in IC_{50} over the lead compound NSAH (**TP8**) (Figure 5 and Table 1). A few of the compounds were also studied in other cell lines (A549 and HCT-116), showing similar potency as in Panc1 cells (Supplemental Figure 3). This finding suggests that these compounds do not target Panc1 cells specifically, but may be universally active against cancer cells, as would be expected since RR is found in all cells.

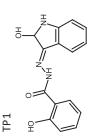
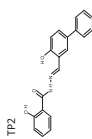
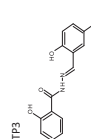
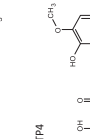
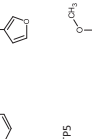
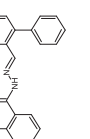
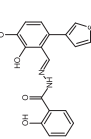
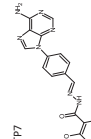
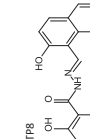
Discussion and conclusions

Decades of effort have been invested into elucidating the structure and physiological function of ribonucleotide reductase, in

order to better target inhibitors for therapeutic intervention. While numerous diverse inhibitors have been developed to target hRR and several have been approved for clinical use, there have been few successful attempts to identify a non-nucleoside reversible inhibitor that targets the large subunit of hRR. In a recent paper by Ahmad *et al.*, we reported on a rapid moderate-throughput screen that identified the first non-nucleoside inhibitor binding to the C-site, NSAH^{35,36}. In a subsequent study by Huff *et al.*, a library of compounds was produced, replacing the substituents on either side of the hydrazone moiety of NSAH with polar substituents to examine their effects on activity³⁷. It was determined that replacing the phenol with polar substituents in the ortho position achieved the best activity against hRR. Replacement of the naphthalene with an indole provided similar activity. It was concluded that these derivatives favoured the C-site, just like NSAH, and all derivatives that showed improved activity against hRR in comparison to NSAH had increased interactions in the phosphate-binding site. However, these compounds had limited cellular activity.

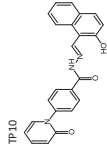
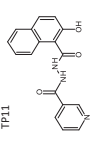
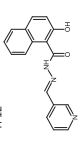
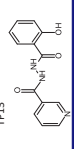
Using the co-crystal structure of NSAH bound at the C-site of hRRM1 and its interactions (PDB code 5TUS) as a template in the

Table 1. Summary of experimental data and molecular docking and pharmacokinetic data derived from the Schrödinger software.

Chemical structure	Name	Molecular weight	Measured KD (μM)	Corrected KD (μM)	Cell based IC50 (μM)	Docking Score	LogP (o/w)	Membrane permeability: caco-2 (nm/sec)	Membrane permeability: MDCK (nm/sec)	Rotatable bonds	Hydrogen bond acceptors	Hydrogen bond donors
Group 1												
	(E)-2-hydroxy-N'-(2-oxindolin-3-ylidene)benzohydrazide	281.08	14.97 \pm 1.8	6.2 \pm 0.77	>10	-6.055	2.556	191	82	4	3.25	1
	(E)-2-hydroxy-N'-(4-hydroxy-[1,1'-biphenyl]-3-yl)methylene)benzohydrazide	332.12	36.02 \pm 3.4	8.7 \pm 2.4	2.400	-6.294	4.163	358	163	7	3	2
	(E)-2-hydroxy-N'-(2-hydroxy-5-(thiophen-3-yl)benzylidene)benzohydrazide	338.07	53.81 \pm 8.0	5.3 \pm 1.42	2.316	-6.613	4.04	358	330	6	3	2
	(E)-N'-(6-(furan-3-yl)-2-hydroxy-3-methoxybenzylidene)-2-hydroxybenzohydrazide	352.11	31.48 \pm 1.7	9.3 \pm 0.56	0.765	-6.025	3.534	458	213	7	4.25	2
	(E)-2-hydroxy-N'-(3-hydroxy-4-methoxy-[1,1'-biphenyl]-2-yl)methylene)benzohydrazide	362.13	35.44 \pm 1.9	4.8 \pm 0.33	1.461	-6.451	4.33	442	205	8	3.75	2
	(E)-2-hydroxy-N'-(2-hydroxy-3-methoxy-6-(thiophen-3-yl)benzylidene)benzohydrazide	368.08	30.0 \pm 5.0	9.4 \pm 1.6	0.393	-6.461	4.29	437	406	7	3.75	2
	(E)-N'-(4-(6-amino-9H-purin-9-yl)benzylidene)-2-hydroxybenzohydrazide	373.13	19.30 \pm 1.96	4.0 \pm 1.06	>10	-7.816	2.404	65	26	6	6.25	3
	(E)-2-hydroxy-N'-(2-hydroxynaphthalen-1-yl)methylene)benzohydrazide	306.32	31.29 \pm 2.8	22.0 \pm 5.67	1.075	-6.293 (cis)	3.505	471	219	6	3	2
Group 2												
	2-(5-(4-methoxyphenyl)thiazol-2-yl)phenol	283.34	70.16 \pm 8.8	9.9 \pm 2.07	>20	-6.764	3.799	3064	2325	2	3	1

(continued)

Table 1. Continued.

Chemical structure	Name	Molecular weight	Measured KD (μM)	Corrected KD (μM)	Cell based IC50 (μM)	Docking Score	LogP (o/w)	Membrane permeability: caco-2 (nm/sec)	Membrane permeability: MDCK (nm/sec)	Rotatable bonds	Hydrogen bond acceptors	Hydrogen bond donors
	(E)-N'-(2-hydroxynaphthalen-1-yl)methylene)-4-(2-oxopyridin-1(2H)-yl)benzohydrazide	383.13	36.76 \pm 2.0	9.7 \pm 1.36	2.920	-5.907	3.707	351	160	5	6.25	2
	N'-(2-hydroxy-1-naphthoyl)nicotinothiazide	307.31	89.65 \pm 4.9	4.1 \pm 0.24	>10	-5.969	2.73	277	124	4	4.75	0.5
	(E)-2-hydroxy-N'-(pyridin-3-ylmethylene)-1-naphthohydrazide	291.30	27.44 \pm 2.0	16.3 \pm 1.3	>10	-5.230	3.362	620	295	5	3.75	1
	N'-(2-hydroxybenzoyl)nicotinothiazide	257.25	60.62 \pm 3.1	2.9 \pm 0.39	>10	-5.335	1.75	218	95	4	4.75	0.5

present study, a small library of compounds was designed to increase the interactions with the C-site (Figure 2). It was anticipated that improved interactions would strengthen the specificity towards hRR and reduce off-target binding. The library consists of two distinct groups. For the Group 1 compounds, the naphthalene of NSAH was replaced in anticipation of creating more interactions with the residues that are important in binding the phosphates of the natural substrates (termed phosphate-binding site). For the Group 2 compounds, the hydrazine linker was modified and polar groups were added to these linkers. In order to determine how these modifications affected interaction with hRR, computational docking and experimental assays were conducted.

To determine the extent of binding of these compounds to the hRRM1 subunit, quenching of the fluorescence of the internal tryptophans of hRRM1 was measured. The K_D 's ranged from 2.9 ± 0.39 – $22.0 \pm 5.67 \mu\text{M}$, indicating that all of the modified compounds bind more tightly than does NSAH (K_D $22.0 \pm 5.67 \mu\text{M}$) (Table 1). Examination of the docking of these compounds suggests that the overall decrease in K_D is influenced by the predicted increase in interactions with the phosphate-binding site within the C-site of hRRM1 compared to the binding of NSAH. With the exception of **TP3**, all other analogues have stronger interactions with the phosphate-binding site than NSAH (Figure 3(B–D), Supplemental Figure 1(A–I), Supplemental Figure 2(A–M)). Apart from the increase in binding to the phosphate-binding region, no other single binding characteristic explains the trends in relative affinity seen with these 13 compounds; rather, a collection of interactions contribute to the observed binding pattern. All of the compounds with a K_D less than $6.2 \mu\text{M}$ are predicted to make at least one strong hydrogen bond that could contribute to the tight binding to hRRM1. Within this group, **TP7** and **11** are predicted to have the most hydrogen bonds, leading to stronger binding to hRRM1 (Figure 3(C) and Supplemental Figure 1(H)). **TP7** has hydrogen bonds scattered throughout the length of the compound, interacting with the phosphate-binding site, at Cys218 and Ser217, and near loop 2 (Figure 3(C)). Our previous predictions for optimising interactions at the phosphate-binding site and with loop 2 appears to be validated by this study. **TP11** and **13** are the only compounds in this library that have a linker composed of single bonds, allowing for free rotation (Figure 2(B)). With a few exceptions, compounds with a K_D less than $9.4 \mu\text{M}$ form multiple predicted hydrogen bonds. **TP3** is one of the exceptions, making fewer strong interactions than NSAH, and not interacting with the phosphate-binding site (Figure 3(A) and Supplemental Figure 2(C)). **TP3**'s lack of interactions with the phosphate-binding site is compensated by stronger interactions near loop 2. The trend that emerges from the study of this library is that the best hRRM1 binding compounds are either small and flexible (**TP1**, **11**, **13**) or long enough to reach loop 2 and/or the phosphate-binding site (**TP3–7**). Both of these groups of compounds' options contain polar substituents, but there is a limit to the benefit of size and polarity, because some of the larger molecules had low solubility in the aqueous medium of the fluorescence assay.

A common challenge in drug development is that interaction with a target and inhibitory activity against a cell-free enzyme does not always predict how the drug will perform when tested in a cell or animal model. Thus, another approach we employed was to query the structures of the compounds in our library using QikProp, an algorithm of the Schrödinger suite to predict the cell permeability of these compounds in Caco-2 and MDCK cells (Table 1)⁴³. With some exceptions, the algorithm was useful in predicting which compounds might be the most effective against

Panc1 cells. With the exception of **TP1** and **7**, group 1 had the greatest potency in Panc1 cells with IC_{50} 's below $2.5\ \mu\text{M}$ (Figure 5 and Table 1). **TP6**, which had the greatest potency, had the greatest predictable permeability for both Caco-2 and MDCK cells within the top seven compounds (Table 1). **TP4–6** and **8** have similar predicted permeabilities, with the exception of **TP6**, which has a greater permeability for MDCK cells (Table 1). The compounds with IC_{50} 's between 2 and $3\ \mu\text{M}$ are predicted to be less permeable than **TP4–6** and **8** (Table 1). Out of the compounds that had cellular IC_{50} 's greater than $10\ \mu\text{M}$ (**TP1**, **7**, **9**, **11–13**) only **T9** and **12** had good predicted permeability, even greater than that of **TP6** (Table 1). These results suggest that theoretical prediction of permeability does not always predict activity in cells. The lack of activity against cells could be due to an assortment of factors, including poor cell permeability, drug metabolism in the cell rendering them inactive, or being good substrates for efflux pumps.

TP4–6, which were the most potent against growth of Panc1 cells, have very similar structures (Figure 2(B)). These compounds maintain the phenol and the hydrazine linker of NSAH, but in place of the naphthalene is a guaiacol methoxyphenol linked to a furan, benzene, or thiophene. The docking of these compounds to the hRRM1 C-site provides evidence that they bind similarly to each other, revealing the importance of this modification. To further examine this modification and its contribution to enhanced binding and cellular potency, **TP2** and **3** were compared. **TP2** and **3** mimic **TP5** and **6**, respectively, but lack the methoxy group on the guaiacol methoxyphenol (Figure 2(B)). The removal of the methoxy appears to cause over a 2-fold decrease in potency in cells as well as the loss of a similar docking pattern (Table 1, Supplemental Figure 1(B) and Figure 3(A)). In the study by Huff *et al.*, a few compounds contained a methoxy group, although on a different position, which caused a similar type of docking pattern³⁷. However, while the methoxy seems to be an important entity and might be essential for better potency, it does not do so alone. **TP9**, which contains a methoxy group on a benzene ring, is not only ineffective in Panc1 cells but also has a completely different predicted pattern of binding to the C-site (Figure 5, Table 1 and Supplemental Figure 1(E) and 2(I)). This suggests that methoxylation of the benzene ring aids in improving cell and enzyme potency but acts in concert with other polar entities. The addition of the hydroxyls as well as the polar rings aids in the increase in potency. Considering the effects of **TP4–6** in the cells, it might be suggested that a polar ring with an electronegative element might further increase the relative potency.

It is well known that phenolics have potentials for being chemotherapeutic agents; however, these compounds often have poor bioavailability *in vivo*⁴⁴. Typically, phenolics are easily oxidised, leaving them vulnerable to chemical degradation or bacterial decomposition in the GI tract, most commonly by glucuronidation and sulphation. **TP1–8**, **13** contain phenolic acids, which proposes a risk of poor bioavailability when administered *in vivo*, eliminating an oral administration and restricting it to IV administration. As an oral compound is more desirable for patients for its ease of use, it might be beneficial to modify these compounds if they exhibit poor bioavailability in mouse studies. Modifying these compounds by converting the phenolic to esters or ethers might produce a pro-drug and increase the bioavailability of the phenolic metabolites.

A PAINS filter (<http://cbligand.org/PAINS/>), which is a now well-defined way to identify the presence of potentially problematic functional groups in analogue design, was used on our compound library. Despite our lead compound, NSAH, being a potential

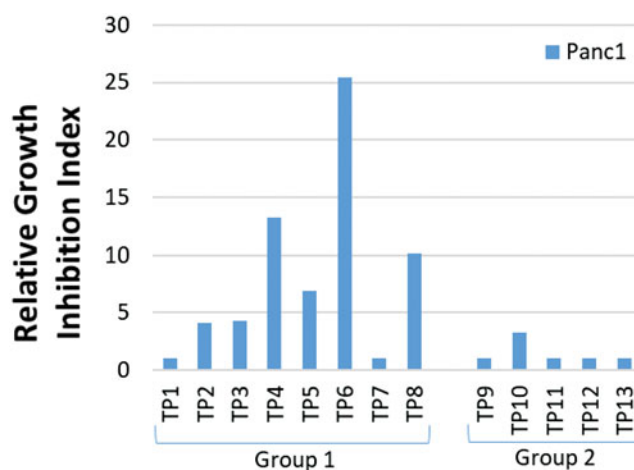


Figure 5. Cancer growth-inhibitory activity of Panc1 pancreatic cancer cell line by TP compounds.

PAINS candidate, our studies have validated this compound as an RR inhibitor binding to the C-site of hRR1 and inhibiting RR in cells^{35,37}. This validation adds confidence that **TP1–13** would bind to the hRR1 C-site as docking to this site displayed favourable poses and possibly inhibits RR in cells. When developing compounds against RR, there is always a concern that these compounds contain chelating properties that may affect the Fe and free radical housed in the small subunit, a crucial element needed for the activity of RR. There have been many reports of agents that inhibit RR by this mechanism^{32,45–49}. As this was a concern, NSAH was tested for its ability to chelate metals³⁷. Results indicated that NSAH does not chelate Fe^{3+} , the iron form present in RR, up to concentrations of 5 mM nor does it bind or sequester Mg^{2+} ions, which are also critical for RR activity. As these concerns are not an issue for the lead compound NSAH, we predict that these will not be an issue with **TP1–13** either.

It is generally understood that targeting RR for cancer therapeutics is a challenging task as RR is present in all cells, normal and malignant. We have previously shown that the lead compound NSAH (**TP8**) was much less effective against blood progenitor cells than against cancer cell lines, demonstrating that NSAH has a higher therapeutic index than gemcitabine in the same cell-cell comparison³⁵. This suggests that NSAH has selective activity in malignant cells, exploiting the greater proliferation in cancer cells⁵⁰. Accordingly, the new class of inhibitors designed from NSAH might provide a superior, safer anticancer treatment. Results from this study indicate that replacing the naphthalene ring of NSAH with other cyclic ring structures containing methoxy and polar constituents results in analogues with superior activity against cancer cells. Future studies will elucidate cyclic and polar constituents which may provide further improvements in this class of RR inhibitors.

Acknowledgements

The authors thank Dr. William E. Harte (School of Medicine, CWRU) for insightful comments and suggestions during the development of this project. The authors thank Drs. J. Mieyal, R. Viswanathan, S. Huff, M. Kumar, and D. Wald, for useful discussions. This work made use of the High Performance Computing Resource in the Core Facility for Advanced Research Computing at Case Western Reserve University.

Disclosure statement

The authors report no declarations of interest and also declare no competing financial interest.

Funding

This study was supported by NIH funding to P.I.: Dr. Chris G. Dealwis (R01GM100887), Case Comprehensive Cancer Centre CTSC pilot grant and Council to Advance Human Health. Drs. Lee and Dealwis were funded by the Taipei Medical School, Taiwan-CWRU grant. This research was supported in part by the Translational Research Shared resource of the Case Comprehensive Cancer Centre (P30CA043703) and Center for Scientific Review.

ORCID

Tessianna A. Misko  <http://orcid.org/0000-0002-9270-7382>

References

- Brown NC, Reichard P. Role of effector binding in allosteric control of ribonucleoside diphosphate reductase. *J Mol Biol* 1969;46:39–55.
- Stubbe J, Ge J, Yee CS. The evolution of ribonucleotide reduction revisited. *Trends Biochem Sci* 2001;26:93–9.
- Jordan A, Reichard P. Ribonucleotide reductases. *Annu Rev Biochem* 1998;67:71–98.
- Kolberg M, Strand KR, Graff P, Andersson KK. Structure, function, and mechanism of ribonucleotide reductases. *Biochim Biophys Acta* 2004;1699:1–34.
- Weinberg G, Ullman B, Martin DW, Jr. Mutator phenotypes in mammalian cell mutants with distinct biochemical defects and abnormal deoxyribonucleoside triphosphate pools. *Proc Natl Acad Sci USA* 1981;78:2447–51.
- Kunz BA, Kohalmi SE, Kunkel TA, et al. International Commission for Protection Against Environmental Mutagens and Carcinogens. Deoxyribonucleoside triphosphate levels: a critical factor in the maintenance of genetic stability. *Mutat Res* 1994;318:1–64.
- Huang M, Zhou Z, Elledge SJ. The DNA replication and damage checkpoint pathways induce transcription by inhibition of the Crt1 repressor. *Cell* 1998;94:595–605.
- Yao R, Zhang Z, An X, et al. Subcellular localization of yeast ribonucleotide reductase regulated by the DNA replication and damage checkpoint pathways. *Proc Natl Acad Sci USA* 2003;100:6628–33.
- Zhao X, Muller EG, Rothstein R. A suppressor of two essential checkpoint genes identifies a novel protein that negatively affects dNTP pools. *Mol Cell* 1998;2:329–40.
- Brown NC, Canellakis ZN, Lundin B, et al. Ribonucleoside diphosphate reductase. Purification of the two subunits, proteins B1 and B2. *Eur J Biochem* 1969;9:561–73.
- Holmgren A, Reichard P, Thelander L. Enzymatic synthesis of deoxyribonucleotides, 8. The effects of ATP and dATP in the CDP reductase system from *E. coli*. *Proc Natl Acad Sci USA* 1965;54:830–6.
- Jordheim LP, Guittet O, Lepoivre M, et al. Increased expression of the large subunit of ribonucleotide reductase is involved in resistance to gemcitabine in human mammary adenocarcinoma cells. *Mol Cancer Ther* 2005;4:1268–76.
- Jordheim LP, Seve P, Tredan O, Dumontet C. The ribonucleotide reductase large subunit (RRM1) as a predictive factor in patients with cancer. *Lancet Oncol* 2011;12:693–702.
- Shao J, Zhou B, Chu B, Yen Y. Ribonucleotide reductase inhibitors and future drug design. *Curr Cancer Drug Targets* 2006;6:409–31.
- Stearns B, Losee KA, Bernstein J. Hydroxyurea. A new type of potential antitumour agent. *J Med Chem* 1963;6:201.
- Donehower RC. An overview of the clinical experience with hydroxyurea. *Semin Oncol* 1992;19:11–9.
- Huang P, Chubb S, Plunkett W. Termination of DNA synthesis by 9-beta-D-arabinofuranosyl-2-fluoroadenine. A mechanism for cytotoxicity. *J Biol Chem* 1990;265:16617–25.
- Heinemann V, Xu YZ, Chubb S, et al. Inhibition of ribonucleotide reduction in CCRF-CEM cells by 2',2'-difluorodeoxycytidine. *Mol Pharmacol* 1990;38:567–72.
- Parker WB, Shaddix SC, Chang CH, et al. Effects of 2-chloro-9-(2-deoxy-2-fluoro-beta-D-arabinofuranosyl)adenine on K562 cellular metabolism and the inhibition of human ribonucleotide reductase and DNA polymerases by its 5'-triphosphate. *Cancer Res* 1991;51:2386–94.
- Parker WB, Shaddix SC, Rose LM, et al. Comparison of the mechanism of cytotoxicity of 2-chloro-9-(2-deoxy-2-fluoro-beta-D-arabinofuranosyl)adenine, 2-chloro-9-(2-deoxy-2-fluoro-beta-D-ribofuranosyl)adenine, and 2-chloro-9-(2-deoxy-2,2-difluoro-beta-D-ribofuranosyl)adenine in CEM cells. *Mol Pharmacol* 1999;55:515–20.
- Griffig J, Koob R, Blakley RL. Mechanisms of inhibition of DNA Synthesis by 2-chlorodeoxyadenosine in human lymphoblastic cells. *Cancer Res* 1989;49:6923–8.
- Avery TL, Rehg JE, Lumm WC, et al. Biochemical pharmacology of 2-chlorodeoxyadenosine in malignant human hematopoietic cell lines and therapeutic effects of 2-bromodeoxyadenosine in drug combinations in mice. *Cancer Res* 1989;49:4972–8.
- Xie C, Plunkett W. Metabolism and actions of 2-chloro-9-(2-deoxy-2-fluoro-beta-D-arabinofuranosyl)-adenine in human lymphoblastoid cells. *Cancer Res* 1995;55:2847–52.
- King RS. Gemcitabine. New first-line therapy for pancreatic cancer. *Cancer Pract* 1996;4:353–4.
- Baker CH, Banzon J, Bollinger JM, et al. 2'-Deoxy-2'-methylcystidine and 2'-deoxy-2',2'-difluorocytidine 5'-diphosphates: potent mechanism-based inhibitors of ribonucleotide reductase. *J Med Chem* 1991;34:1879–84.
- Gandhi V, Plunkett W. Modulatory activity of 2',2'-difluorodeoxycytidine on the phosphorylation and cytotoxicity of arabinosyl nucleosides. *Cancer Res* 1990;50:3675–80.
- Wang J, Lohman GJ, Stubbe J. Enhanced subunit interactions with gemcitabine-5'-diphosphate inhibit ribonucleotide reductases. *Proc Natl Acad Sci USA* 2007;104:14324–9.
- Heinemann V, Schulz L, Issels RD, Plunkett W. Gemcitabine: a modulator of intracellular nucleotide and deoxynucleotide metabolism. *Semin Oncol* 1995;22:11–8.
- Heinemann V, Xu YZ, Chubb S, et al. Cellular elimination of 2',2'-difluorodeoxycytidine 5'-triphosphate: a mechanism of self-potential. *Cancer Res* 1992;52:533–9.
- Honeywell RJ, Ruiz van Haperen VW, Veerman G, et al. Inhibition of thymidylate synthase by 2',2'-difluoro-2'-deoxycytidine (Gemcitabine) and its metabolite 2',2'-difluoro-2'-deoxyuridine. *Int J Biochem Cell Biol* 2015;60:73–81.
- Heinemann V. Ongoing selective internal radiation therapy-based studies in the treatment of liver-dominant metastatic

- colorectal cancer. *Future Oncol* (London, England) 2014;10:37–9.
32. Heinemann V, Plunkett W. Modulation of deoxynucleotide metabolism by the deoxycytidylate deaminase inhibitor 3,4,5,6-tetrahydrodeoxyuridine. *Biochem Pharmacol* 1989;38:4115–21.
 33. Pourquier P, Gioffre C, Kohlhagen G, et al. Gemcitabine (2',2'-difluoro-2'-deoxycytidine), an antimetabolite that poisons topoisomerase I. *Clin Cancer Res* 2002;8:2499–504.
 34. Pourquier P, Pilon AA, Kohlhagen G, et al. Trapping of mammalian topoisomerase I and recombinations induced by damaged DNA containing nicks or gaps. Importance of DNA end phosphorylation and camptothecin effects. *J Biol Chem* 1997;272:26441–7.
 35. Ahmad MF, Alam I, Huff SE, et al. Potent competitive inhibition of human ribonucleotide reductase by a nonnucleoside small molecule. *Proc Natl Acad Sci USA* 2017;114:8241–6.
 36. Ahmad MF, Huff SE, Pink J, et al. Identification of non-nucleoside human ribonucleotide reductase modulators. *J Med Chem* 2015;58:9498–509.
 37. Huff SE, Mohammed FA, Yang M, et al. Structure-guided synthesis and mechanistic studies reveal sweetspots on naphthyl salicyl hydrazone scaffold as non-nucleosidic competitive, reversible inhibitors of human ribonucleotide reductase. *J Med Chem* 2018;61:666–80.
 38. Fairman JW, Wijerathna SR, Ahmad MF, et al. Structural basis for allosteric regulation of human ribonucleotide reductase by nucleotide-induced oligomerization. *Nat Struct Mol Biol* 2011;18:316–22.
 39. Labarca C, Paigen K. A simple, rapid, and sensitive DNA assay procedure. *Anal Biochem* 1980;102:344–52.
 40. Friesner RA, Banks JL, Murphy RB, et al. Glide: a new approach for rapid, accurate docking and scoring. 1. Method and assessment of docking accuracy. *J Med Chem* 2004;47:1739–49.
 41. Halgren TA, Murphy RB, Friesner RA, et al. Glide: a new approach for rapid, accurate docking and scoring. 2. Enrichment factors in database screening. *J Med Chem* 2004;47:1750–9.
 42. Friesner RA, Murphy RB, Repasky MP, et al. Extra precision glide: docking and scoring incorporating a model of hydrophobic enclosure for protein-ligand complexes. *J Med Chem* 2006;49:6177–96.
 43. Jorgensen WL, Duffy EM. Prediction of drug solubility from structure. *Adv Drug Deliv Rev* 2002;54:355–66.
 44. Gao S, Hu M. Bioavailability challenges associated with development of anti-cancer phenolics. *Mini Rev Med Chem* 2010;10:550–67.
 45. Lepoivre M, Flaman JM, Bobe P, et al. Quenching of the tyrosyl free radical of ribonucleotide reductase by nitric oxide. Relationship to cytostasis induced in tumor cells by cytotoxic macrophages. *J Biol Chem* 1994;269:21891–7.
 46. Szalai VA, Brudvig GW. Reversible binding of nitric oxide to tyrosyl radicals in photosystem II. Nitric oxide quenches formation of the S3 EPR signal species in acetate-inhibited photosystem II. *Biochemistry* 1996;35:15080–7.
 47. Nyholm S, Mann GJ, Johansson AG, et al. Role of ribonucleotide reductase in inhibition of mammalian cell growth by potent iron chelators. *J Biol Chem* 1993;268:26200–5.
 48. Hershko C. Control of disease by selective iron depletion: a novel therapeutic strategy utilizing iron chelators. *Bailliere's Clin Haematol* 1994;7:965–1000.
 49. Lundberg JH, Chitambar CR. Interaction of gallium nitrate with fludarabine and iron chelators: effects on the proliferation of human leukemic HL60 cells. *Cancer Res* 1990;50:6466–70.
 50. Hakansson P, Hofer A, Thelander L. Regulation of mammalian ribonucleotide reduction and dNTP pools after DNA damage and in resting cells. *J Biol Chem* 2006;281:7834–41.